Supporting Information

Thermal Control over Phosphorescence or Thermally Activated Delayed Fluorescence in a Metal–Organic Framework

Huili Sun,[a] Qiangsheng Zhang,[b] Liuli Meng,[a] Zhonghao Wang,[a] Yanan Fan,[a] Marcel Mayor,[ac] Mei Pan*,[a] and Cheng-Yong Su[a]

[a.] *MOE Laboratory of Bioinorganic and Synthetic Chemistry, Lehn Institute of Functional Materials, IGCME, GBRCE for Functional Molecular Engineering, School of Chemistry, Sun Yat-Sen University, Guangzhou 510006 (China)*
[b.] *Hainan Provincial Key Laboratory of Fine Chem, School of Chemistry and Chemical Engineering, Hainan University, Haikou, P. R. China*
[c.] *1) Department of Chemistry, University of Basel (Switzerland), 2) Institute of Nanotechnology (INT), Karlsruhe Institute of Technology (KIT, Germany).*

*E-mail: panm@mail.sysu.edu.cn

1. Experimental Section

Materials and Instrumentations

All reaction materials were obtained from commercial suppliers and used without further purification. IR spectra were recorded using Nicolet/Nexus-670 FT-IR spectrometer in the region of 4000-400 cm^{-1} using KBr pellets. A Mini-Pellet Press of Specac is used to compress the samples. The single-crystal structures were determined by the Rigaku X-ray single-crystal diffraction system SuperNova with monochromator Cu−Kα radiation (λ = 1.54184 Å). PXRD curves were recorded on a Rigaku SmartLab diffractometer (Bragg−Brentano geometry, Cu−Kα 1 radiation, λ = 1.54056 Å). Thermogravimetric analysis (TGA) was performed on a NETZSCH TG209 system in nitrogen and under 1 atm of pressure at a heating rate of 10 °C min^{-1}. NMR spectra were recorded on a JEOL EX270 spectrometer (^{1}H: 400 MHz; ^{13}C: 100 MHz). UV-Vis absorption spectra were recorded using a Shimadzu UV-2450 spectrophotometer. Fluorescence spectra and decay lifetimes were measured by Edinburgh FLS 980 spectrometer. The emission quantum yields were measured by the integrating sphere in the FLS980 spectrophotometer. The two-photon excited fluorescence spectra were obtained using Astrella/OperA Solo femtosecond-laser.

Measurement of TPEF and TPA cross sections: Keeping the testing conditions consistent, TPEF cross sections of **LIFM-SHL-1** and **DTST** were quantified by comparing the TPEF intensities measured in solid state with that of Rhodamine B (RhB) as a reference, and computed from the following equation,

$$\sigma_{TPEF,sample} = \sigma_{TPEF,reference}\frac{I_{sample}N_{reference}}{I_{reference}N_{sample}}$$

Where $\sigma_{TPEF,\ sample}$ and $\sigma_{TPEF,\ reference}$ represents TPEF action cross section for the sample and reference, respectively. The TPEF intensities of the sample (I_{sample}) is compared with that of Rhodamine B (RhB) ($I_{reference}$) and $N_{reference}$ or N_{sample} is the molecular concertation. Then, TPA cross sections were calculated using the equation $\sigma_{TPA}=\sigma_{TPEF}/\Phi$, where σ_{TPEF} and σ_{TPA} are TPEF and TPA cross sections, and Φ is fluorescence quantum yield.

Preparation of composite membrane LIFM-SHL-1@PVDF

The composite membrane LIFM-SHL-1@PVDF was prepared using a slurry method. PVDF (0.1 g) was dissolved in 5 mL DMF to form a clear solution, to which the grinded powder of LIFM-SHL-1 (0.01 g) was added. The mixture was stirred gently until a uniform dispersion was formed. The dispersion was poured onto a glass slide and dried in a vacuum for 30 min at 80 ℃.

X-ray single crystal structural analysis

Single-crystal X-ray diffraction data for **LIFM-SHL-1** was collected on a Rigaku Oxford SuperNova X-RAY diffractometer system equipped with a Cu sealed tube (λ = 1.54178 Å) at 50 kV and 0.80 mA. The structure was solved by direct methods, and refined by full-matrix least-square methods with the SHELXL-2014 program package.[1] All hydrogen atoms were located in calculated positions and refined anisotropically. The crystallographic data for **LIFM-SHL-1** was listed in Table S1. The single crystal data have been deposited in the Cambridge Crystallographic Data Center (CCDC No: 2251129).

Calculation methods

Simulation calculations of **DTST** and **LIFM-SHL-1** fragments were carried out with Gaussian 09 program package.[2] In view of the periodicity and large number of atoms of MOF materials, we intercepted the smallest packing unit in their crystalline cells as the object of study. Since the ligand is the luminophore of the MOF materials, the metal atoms and solvent molecules were discarded. The geometries of all fragments were obtained from the X-ray single-crystal structure measurements of the MOFs. **DTST** and **LIFM-SHL-1** fragments at the level of B3LYP-GD3(BJ)/6-311G** have been evaluated. Time-dependent density functional theory (TD-DFT) calculations were performed based on the optimized molecular structure. Natural transition orbitals (NTOs) analysis and IRI analysis were carried out by Multiwfn software[3-4] and VMD.[5] All orbitals were visuallized by Multiwfn (isovalue = 0.02). The Hirshfeld surfaces and decomposed fingerprint plots were calculated and mapped using CrystalExplorer 21.5 package.[6] The Spin Orbit Coupling (SOC) calculation by using Orca. The calculations of **LIFM-SHL-1** was performed with the periodic density functional theory (PDFT) method using the $Dmol^3$ module using Material Studio software package.[7] The initial configuration was fully optimized based on experimental crystal structures by the

Perdew−Wang (PW91) generalized approximation method with the double numerical basic sets plus polarization function.

Synthesis of the ligand DTST

The synthesis of this compound is based on previous reports.[8] 4,4',4",4"'-((3,6-dicyanobenzene-1,2,4,5-tetrayl)tetrakis(sulfanediyl))tetrabenzoic acid (**DTST**). Tetrachloroterephthalonitrile (200 mg, 0.75 mmol), 4-mercaptobenzoic acid (694 mg, 4.5 mmol) and potassium carbonate (1.66 g, 12 mmol) were added under nitrogen into a 100 mL round bottom flask followed by the addition of dry DMF (10 mL). The solution was stirred at 80 °C for 48 h. Then the reaction was quenched very carefully with 4 M HCl (30 mL), the product precipitated as orange solid. This solid was separated by filtration and washed with distilled water. The product recrystallized in ethanol and was dried under vacuum. (Yield 194 mg, 35%). Molecular formula: $C_{36}H_{20}N_2O_8S_4$. ^{1}H NMR (400 MHz, DMSO-d_6): δ (ppm) 13.05 (s, 4H), 7.85 (d, 8H, J = 12 HZ), 7.36 (d, 8H, J = 8.0 HZ); ^{13}C NMR (100 MHz, DMSO-d_6): δ (ppm) 166.99, 145.43, 140.52, 130.77,130.59, 129.74, 128.01, 114.73. IR (KBr, cm^{-1}): ν = 3626 (m), 2986 (m), 2671 (m), 2555 (m), 2230 (w), 1689 (s), 1585 (s), 1492 (w), 1422 (s), 1326 (s), 1297 (s), 1174 (m), 1122 (m), 1078 (m), 1004 (m), 930 (m), 847 (m), 817 (m), 756 (s), 682 (w), 634 (w), 552 (m), 463 (w).

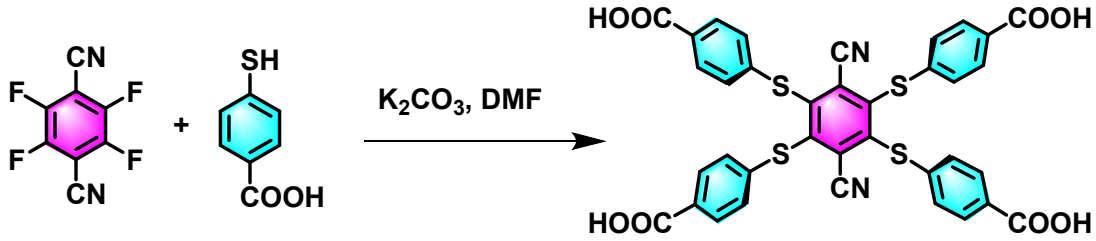

Solvothermal synthesis of LIFM-SHL-1

$Zn(NO_3)_2{\cdot}6H_2O$ (20 mg, 0.08 mmol), **DTST** (7 mg, 0.009 mmol), DMF (2 mL), H_2O (0.2 mL) and HCOOH (40 μL) were placed in a vial (10 mL). The mixture was ultra-sounded for 10 min, and then heated at 100 °C for 1 day. After cooled down to room temperature, yellow bar-shaped crystals with the formula of $(\{Zn(DTST)(DMF)(H_2O)\}_n$ (named as **LIFM-SHL-1**, ~60% yield based on the ligand) was obtained and washed by DMF, separated with filter paper and keep sealed. Elemental analysis calculated for **LIFM-SHL-1**: $C_{39}H_{27}N_3O_{11}S_4Zn_2$: C, 48.16 %; H, 2.80 %; N, 4.32 %; S, 13.19 %; found: C, 52.49 %; H, 2.78 %; N, 4.66 %; S, 13.95 %. Differences may come from the determination of free solvent molecules in crystal structure and the volatilization of the guest solvent molecules. IR (KBr, cm^{-1}): 3376 (m), 2924

(w), 2866 (w), 2219 (w), 1931 (w), 1668 (m), 1586 (s), 1537 (s), 1488 (w), 1414 (s), 1402 (s), 1307 (w), 1278 (w), 1217 (w), 1180 (m), 1152 (w), 1140 (w), 1108 (w), 1014 (m), 860 (w), 843 (w), 776 (s), 744 (w), 702 (w), 665(w), 524 (w).

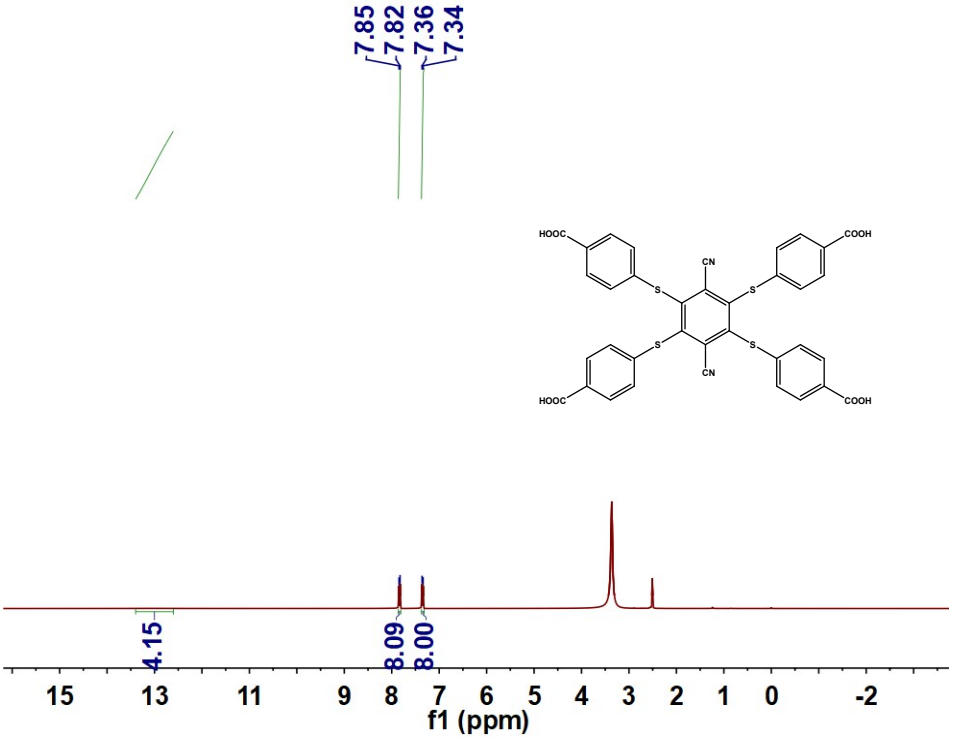

Figure S1. ^{1}H NMR spectrum of **DTST** in DMSO-d_6.

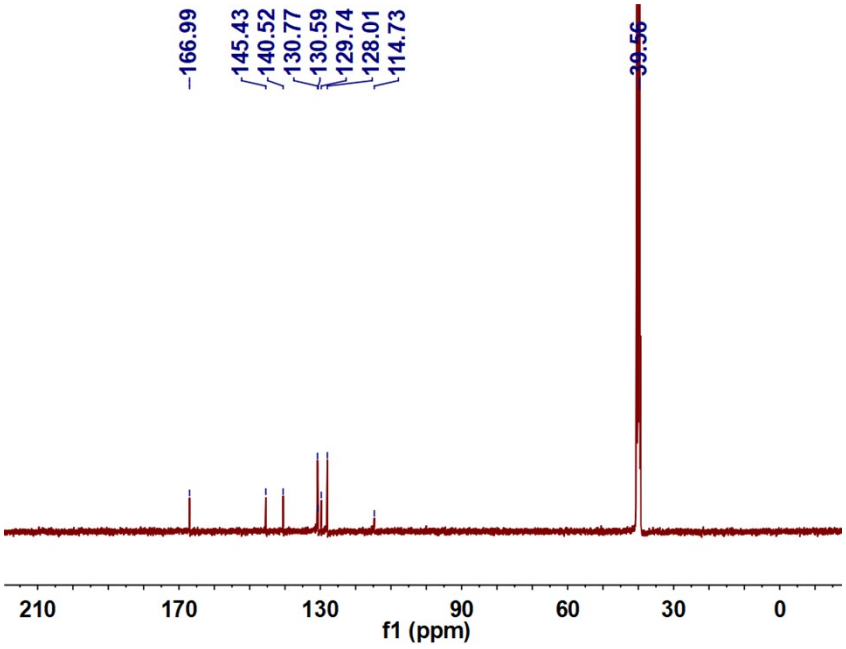

Figure S2. ^{13}C NMR spectrum of **DTST** in DMSO-d_6.

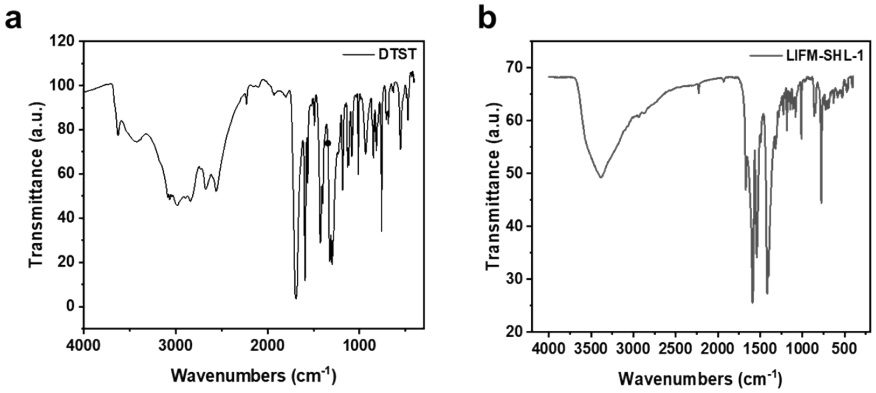

Figure S3. FT-IR spectra of **DTST** and **LIFM-SHL-1**.

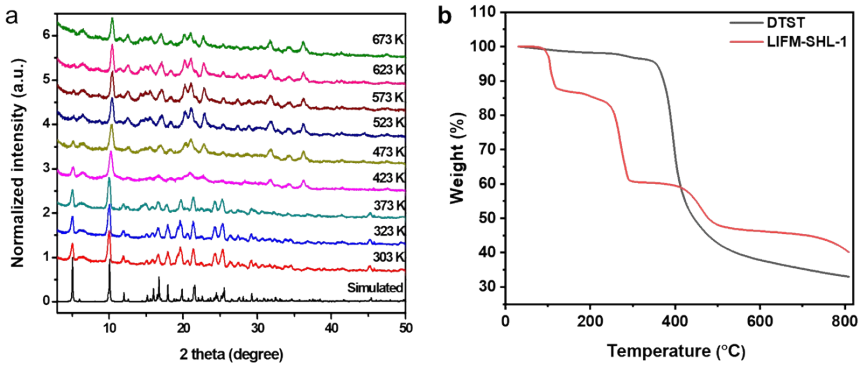

Figure S4. (a) PXRD patterns of **LIFM-SHL-1** heated at different temperature under air atmosphere; (b) TGA curves of ligand **DTST** and **LIFM-SHL-1** under N_2 atmosphere at a heating rate of 10 °C / min.

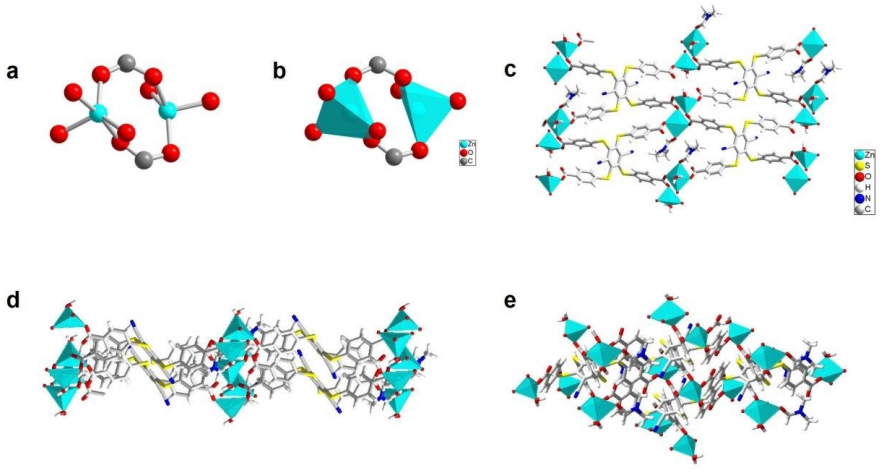

Figure S5. Crystal structure of **LIFM-SHL-1**: (a, b) coordination modes, (c-e) self-assembled 2D model along the *a*-axis, *b*-axis and *c*-axis.

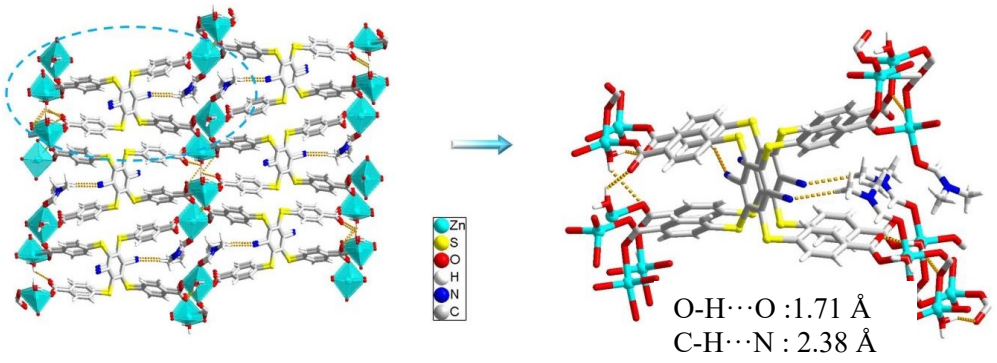

Figure S6. Ligand linked Zn(II) clusters forming a three-dimensional coordination network via intra- and intermolecular interactions in **LIFM-SHL-1**.

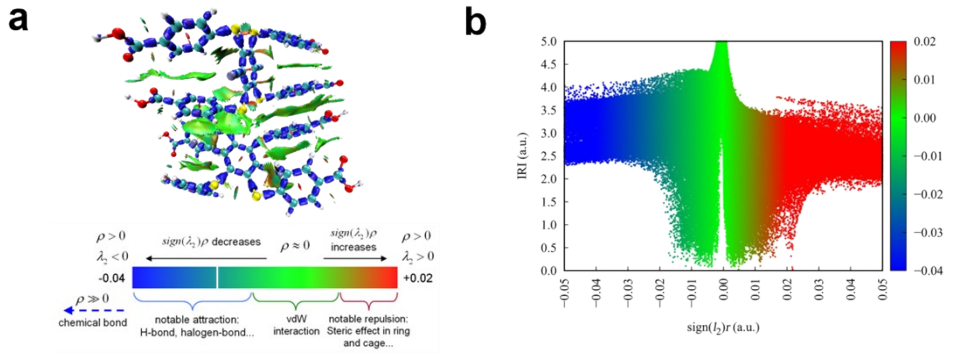

Figure S7. The interaction region indicator (IRI) analysis of (a, b) **LIFM-SHL-1** fragments.

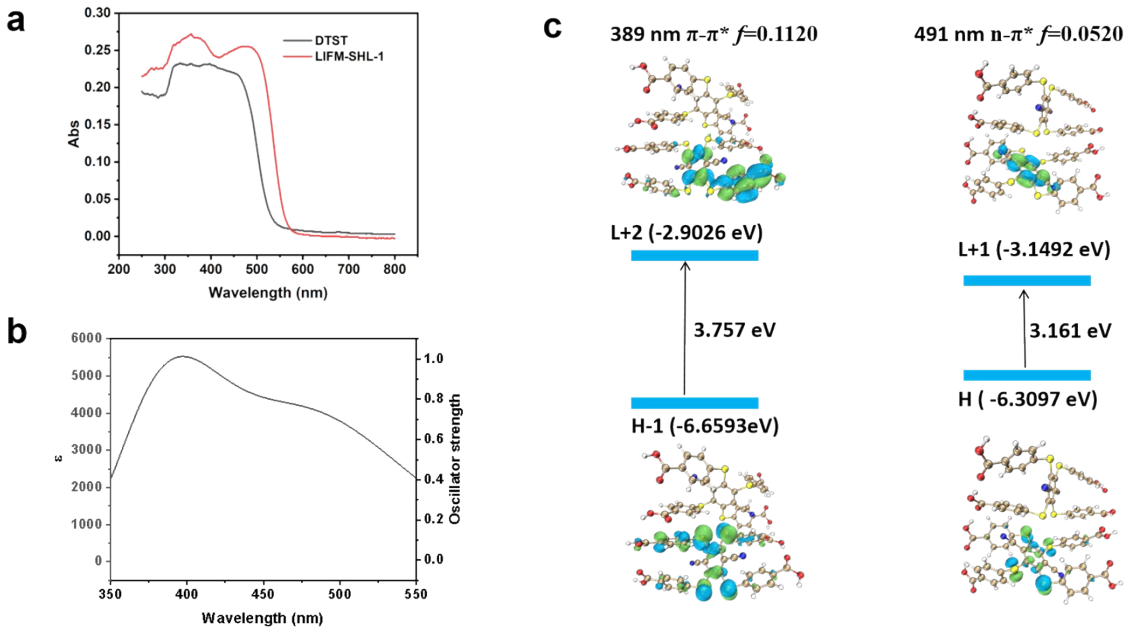

Figure S8. (a) Solid state UV-Visible absorption spectra of ligand DTST and LIFM-SHL-1; The calculated optical absorption spectra (b) and molecular orbital diagrams (c) associated

with the π-π* and n-π* transitions of LIFM-SHL-1.

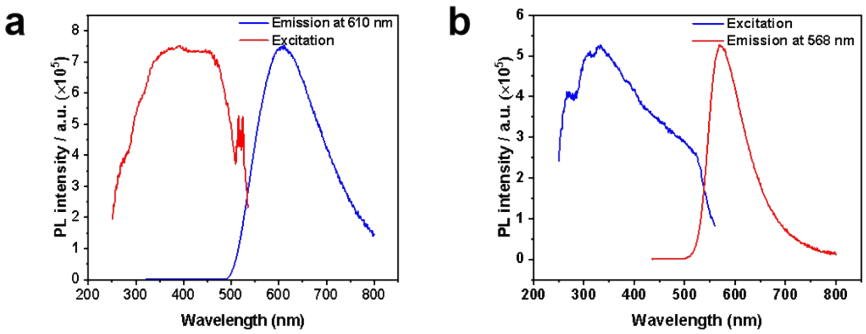

Figure S9. The excitation and emission spectra of **DTST** (a), and **LIFM-SHL-1** (b) at RT.

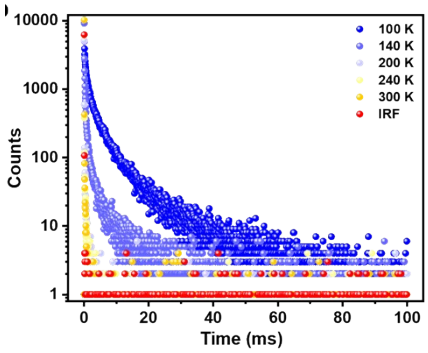

Figure S10. Decay curves of **LIFM-SHL-1** at 100 K−300 K at 600 nm.

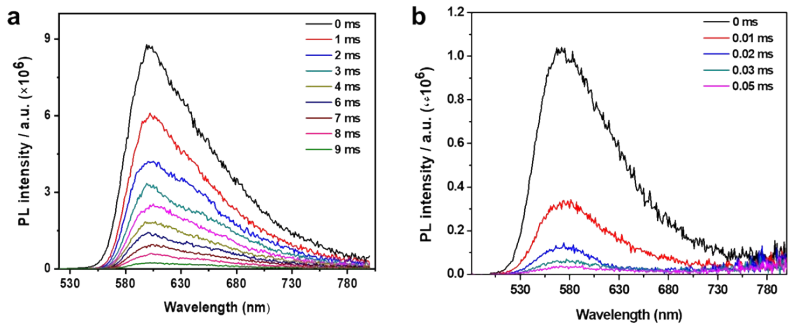

Figure S11. PL spectra of **LIFM-SHL-1** measured at different time intervals and different temperature of 77 K (a) and 300 K (b) after the removal of 365 nm UV light.

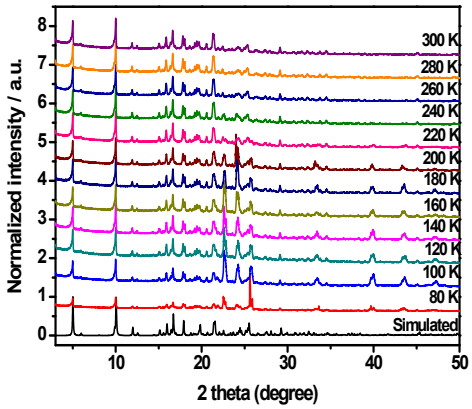

Figure S12. PXRD patterns of **LIFM-SHL-1** heated at different temperature under air atmosphere.

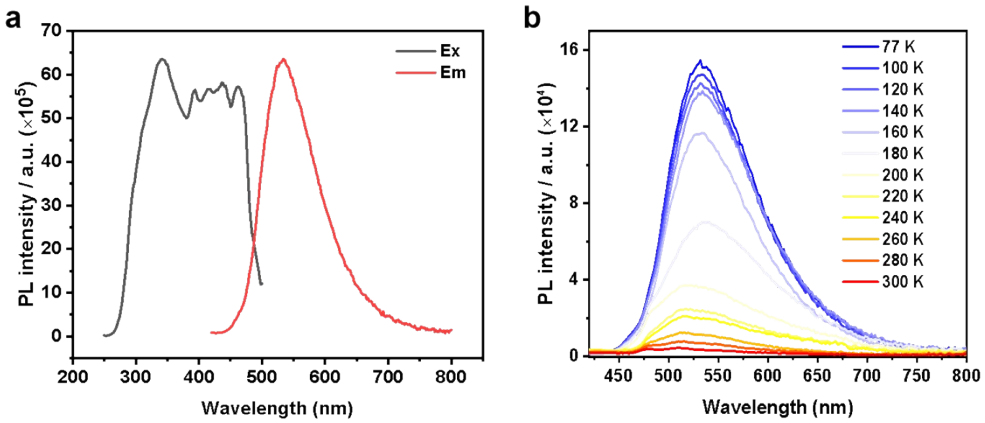

Figure S13. (a) The excitation and emission spectra of **DTST** in 2-methyltetrahydrofuran solution (2-MTHF, 50.0 μM) at RT; (b) Temperature-dependent steady-state PL spectra of **DTST** in 2-MTHF (50.0 μM).

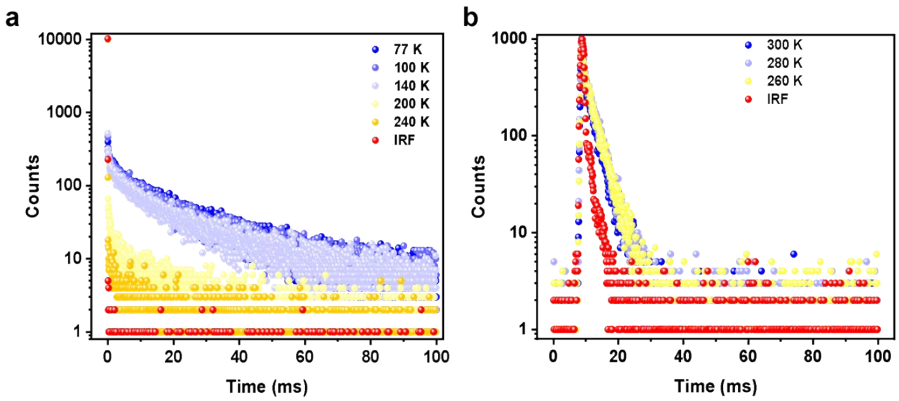

Figure S14. Decay curves of **DTST** in 2-MTHF (50.0 μM) at 77 K−300 K at 530 nm.

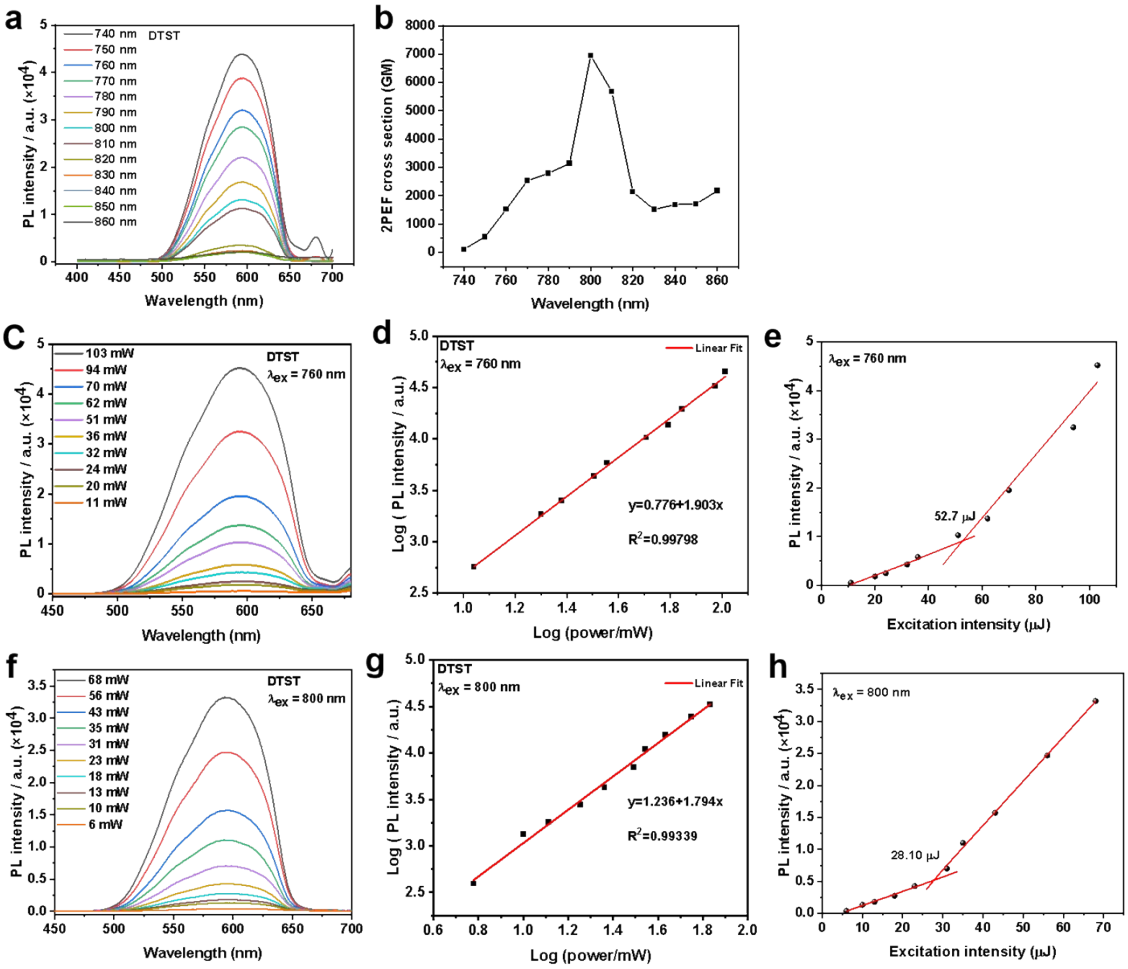

Figure S15. (a) Emission spectra of **DTST** under different two photon excitation wavelength; (b) Excitation wavelength dependent 2PEF cross sections of **DTST**; (c) Power-dependent emission spectra of **DTST** (λ_{ex} = 760 nm); The corresponding Log (PL Intensity)-Log (Power) relationship (d) and the change in slope of emission intensity for threshold determination (e); (f) Power-dependent emission spectra of **DTST** (λ_{ex} = 800 nm); The corresponding Log (PL Intensity)-Log (Power) relationship (g) and the change in slope of emission intensity for threshold determination (h).

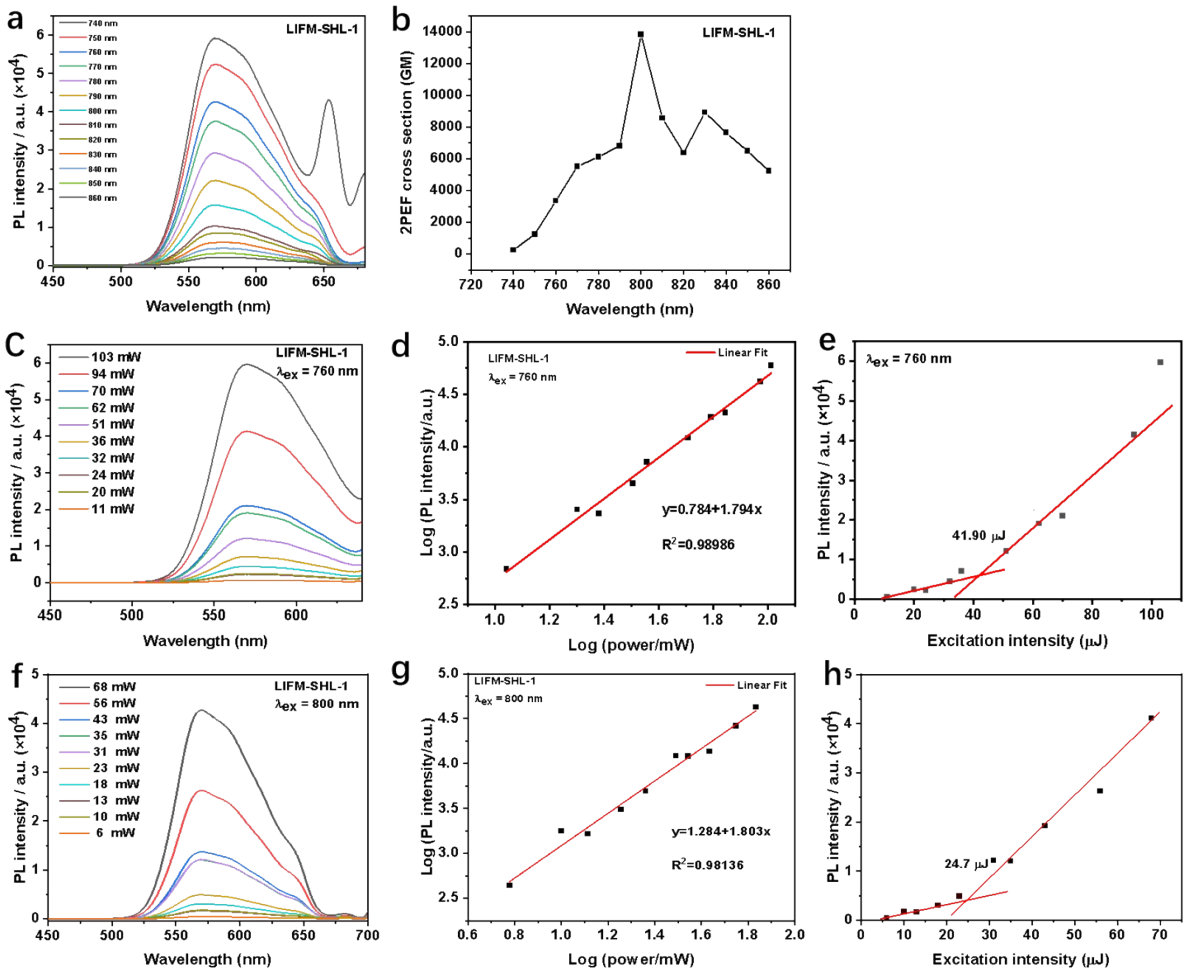

Figure S16. (a) Emission spectra of **LIFM-SHL-1** under different two photon excitation wavelength; (b) Excitation wavelength dependent 2PEF cross sections of **LIFM-SHL-1**; (c) Power-dependent emission spectra of **LIFM-SHL-1** (λ_{ex} = 760 nm); The corresponding Log (PL Intensity)-Log (Power) relationship (d) and the change in slope of emission intensity for threshold determination (e); (f) Power-dependent emission spectra of **LIFM-SHL-1** (λ_{ex} = 800 nm); The corresponding Log (PL Intensity)-Log (Power) relationship (g) and the change in slope of emission intensity for threshold determination (h).

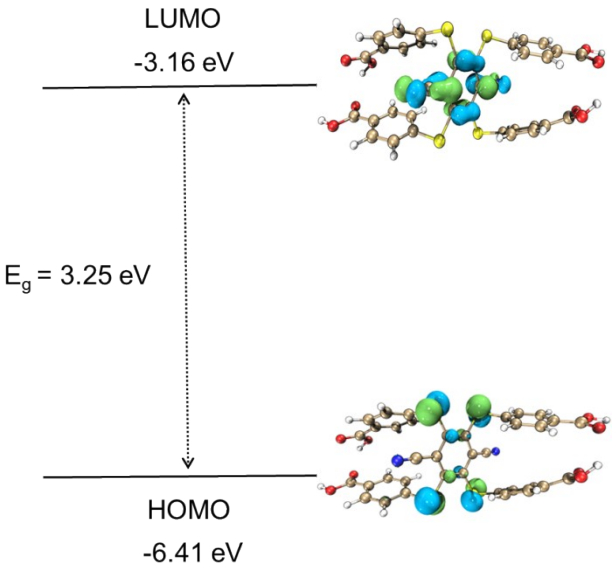

Figure S17. The frontier molecular orbitals (FMOs) of **DTST**.

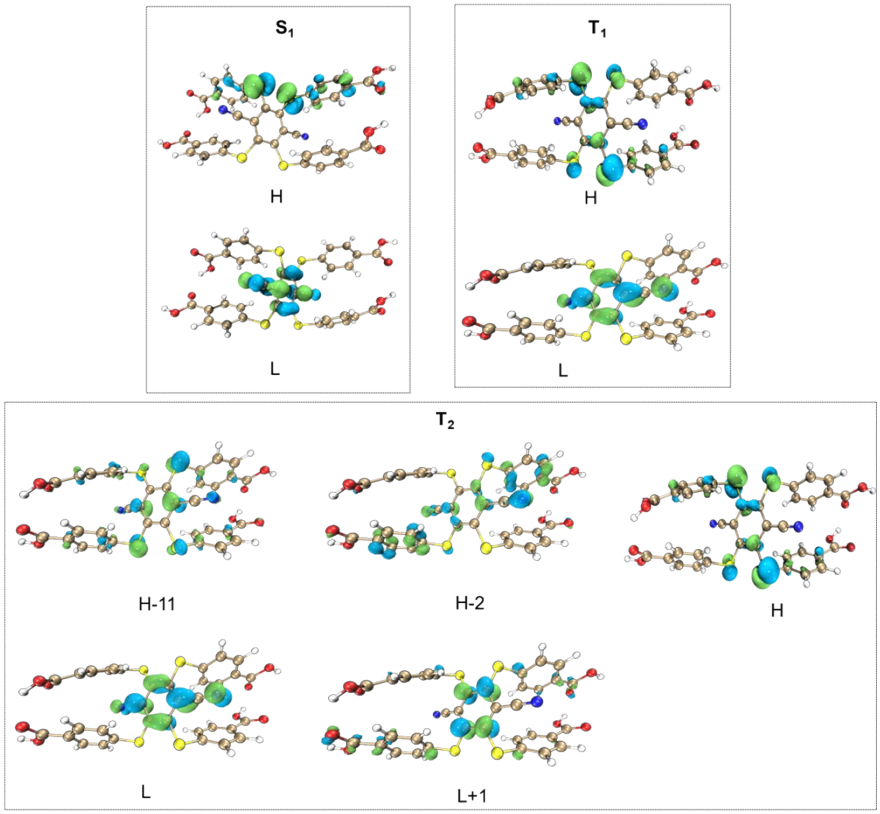

Figure S18. The nature transition orbitals (NTOs) of **DTST**.

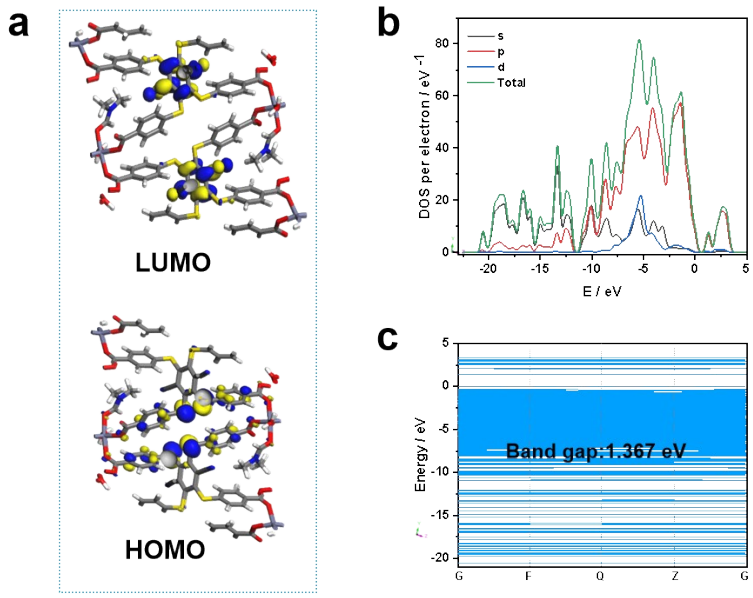

Figure S19. (a) The HOMO/LUMO molecular orbitals, (b) band structures around the Fermi energy level, and (c) total/partial electronic density of states for **LIFM-SHL-1**.

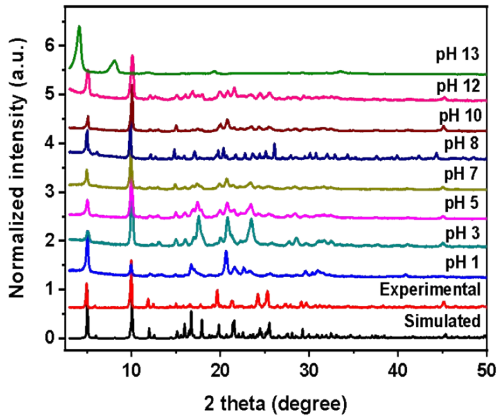

Figure S20. PXRD patterns of **LIFM-SHL-1** in the pristine state and after soaking in acid, and base solution for 12 h.

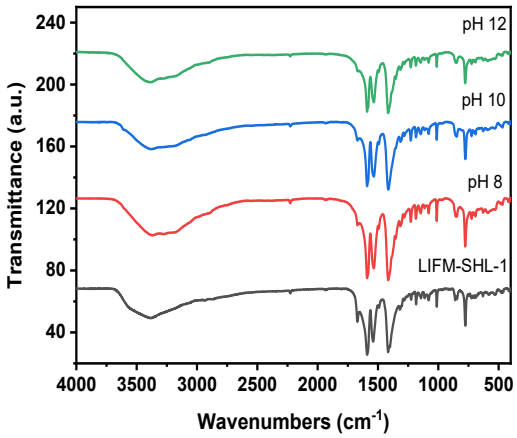

Figure S21. FT-IR spectra of **LIFM-SHL-1** after soaking in base solution.

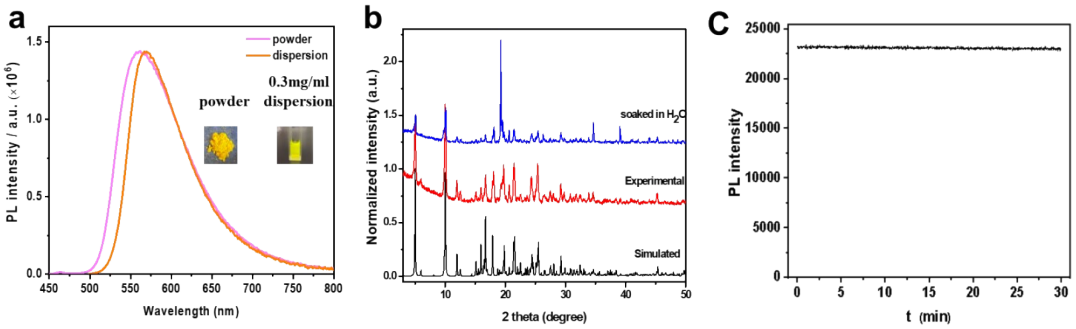

Figure S22. (a) Emission spectra of **LIFM-SHL-1** in solid state and in aqueous dispersion (The inserts show the fluorescence color under UV light); (b) PXRD patterns of **LIFM-SHL-1** soaked in H_2O for 12 h after ultrasonic treatment; (c) Luminescence stability measurements of the **LIFM-SHL-1** dispersions.

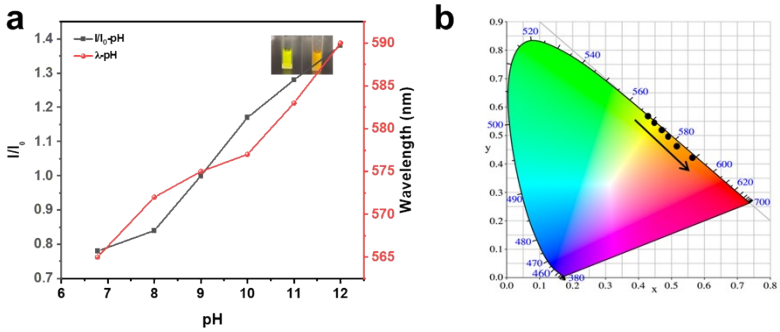

Figure S23. (a) Variation of the emission intensity and peak position of **LIFM-SHL-1** with pH. The insets are the photos of the dispersions at pH 6.7 (left) and pH 11.9 (right) under UV light; (b) The CIE coordinates showing the color variation with pH.

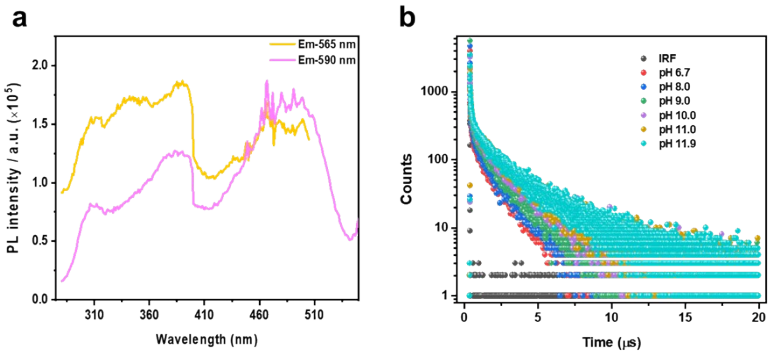

Figure S24. (a) The excitation spectra of **LIFM-SHL-1** measured at the emission wavelengths of at 568 nm (pH 6.7), and 590 nm (pH 11.9); (b) Luminescence decay curves of **LIFM-SHL-1** from pH 6.7 (emission at 568 nm) and pH 11.9 (emission at 590 nm) after photoexcitation at 365 nm.

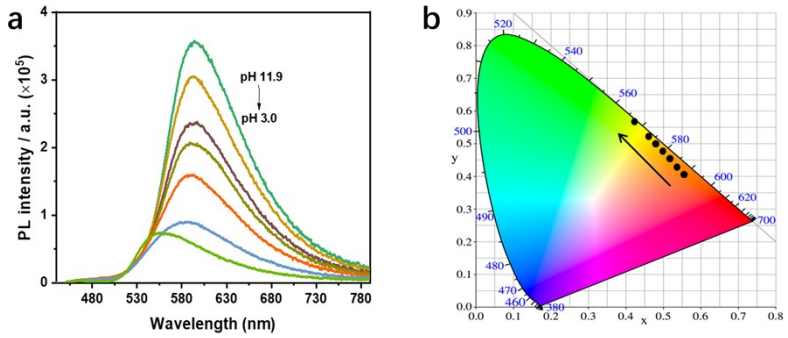

Figure S25. (a) Emission spectra of **LIFM-SHL-1** in aqueous dispersions with pH varying from 11.9 to 3.0; (b) The CIE coordinates showing the color variation with pH.

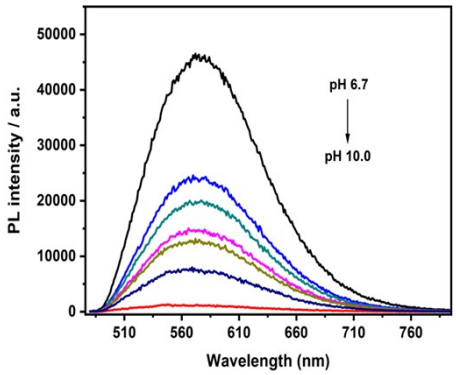

Figure S26. Emission spectra (365 nm excitation) of **DTST** in aqueous dispersions with pH varying from 6.7 to 10.0.

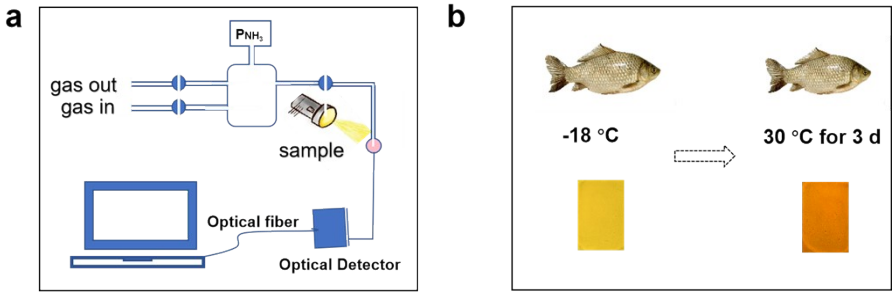

Figure S27. (a) Schematic diagram of NH_3 sensing device with **LIFM-SHL-1; (b)** Schematic diagram of food spoilage detection.

Table S1. Crystal data and structure refinement parameters for **LIFM-SHL-1**.

Compound	**LIFM-SHL-1**
Empirical formula	$C_{39}H_{27}N_3O_{11}S_4Zn_2$
CCDC No.	2251129
Formula weight	972.61
Crystal system	triclinic
Space group	$P\bar{1}$
a/Å	5.9240(3)
b/Å	18.3064(13)
c/Å	18.6104(12)
α/°	106.425(6)
β/°	98.852(5)
γ/°	92.567(5)
Volume/Å^3	1905.5(2)
Z	2
ρ_{calc}g/cm^3	1.695
μ/mm^{-1}	4.182
F(000)	988.0
Radiation	CuK_α (λ = 1.54184)
Data/restraints/parameters	3933/0/536
GooF	1.053
R_2 [I>=2σ (I)]	R_1 = 0.0536, wR_2 = 0.1397
wR_2 [all data]	R_1 = 0.0657, wR_2 = 0.1488

Table S2. The decay lifetimes of **DTST** at 610 nm measured at different temperature.

Temperature/K	τ_1 (ns)	A_1	τ_2 (μs)	A_2	τ (μs)
100	17.80	26.69	7.83	73.31	5.74
140	52.91	10.23	3.16	89.77	2.84
200	24.28	22.73	0.66	77.27	0.52
240	17.27	30.09	0.42	69.91	0.30
300	16.88	38.62	0.27	61.38	0.17

Table S3. The decay lifetime of **LIFM-SHL-1** at 600 nm measured at different temperature.

Temperature/K	τ_1 (μs)	A_1	τ_2 (μs)	A_2	τ (μs)
100	866.65	39.36	6643.07	60.64	4369.47
140	169.06	64.38	2494.58	35.62	997.41
200	36.05	72.85	403.24	27.15	135.74
240	29.22	73.17	341.01	26.83	112.87
300	22.85	82.25	250.72	17.75	63.30

Table S4. The decay lifetime of **LIFM-SHL-1** at 568 nm measured at different temperature.

Temperature/K	τ_p (ns)	A_p (%)	τ_d(μs)	A_d (%)	τ (μs)
200	957.78	42.67	4.03	57.33	2.72
220	882.26	33.61	4.29	66.39	3.14
240	801.82	24.68	4.81	75.32	3.82
260	714.34	17.11	5.98	82.89	5.08
280	347.64	9.96	6.66	90.04	6.03
300	277.20	7.96	8.58	92.04	7.92

Table S5. The photophysical parameters of **LIFM-SHL-1** at room temperature.

Compounds	**LIFM-SHL-1**
Φ_{PL} / %	8.64
Φ_{prompt} / %	0.69
$\Phi_{delayed}$ / %	7.95
τ_{prompt} / ns	277.20
$\tau_{delayed}$ / μs	8.58
A_{prompt} / %	7.96
$A_{delayed}$ / %	92.04
$K_{r,s}$ / 10^4 S^{-1}	2.49
$K_{nr,s}$ / $10^5 S^{-1}$	2.63
K_{RISC} / 10^6 S^{-1}	1.57

The photophysical parameters of **LIFM-SHL-1** are obtained according to the following equations:[9]

$$\Phi_p = \Phi_F A_p \quad (1)$$

$$\Phi_d = \Phi_F A_d \quad (2)$$

$$k_p = 1/\tau_p \quad (3)$$

$$k_d = 1/\tau_d \quad (4)$$

$$K_{r,s} = \Phi_p k_p + \Phi_d k_d \approx \Phi_p k_p \quad (5)$$

$$K_{nr,s} = (1 - \Phi_{PL}) / \Phi_{PL} \times K_{r,s} \quad (6)$$

$$k_{RISC} = \Phi_{PL} / \tau_d \Phi_p \quad (7)$$

Abbreviations: Φ_{PL} = absolute photoluminescence quantum yield; τ_{prompt} and $\tau_{delayed}$ = lifetimes calculated from the prompt and delayed fluorescence decay, respectively; A_{prompt} and $A_{delayed}$ = ratio of prompt component and delayed component and $A_{delayed} = 1 - A_{prompt}$; Φ_{prompt} and $\Phi_{delayed}$ = quantum yields from prompt and delayed components, respectively, determined from the total Φ_{PL} and the proportion of the integrated area of each component in the transient spectra to the total integrated area; The rate constants of radiative decay ($K_{r,s}$) and nonradiative decay ($K_{nr,s}$) from S_1 to S_0 states; Where the K_P and K_d represent the decay rate constants for prompt and delayed fluorescence, respectively; k_{RISC} = rate constant of reverse intersystem crossing.

The absolute photoluminescence quantum yields (Φ) of DTST and LIFM-SHL-1 are 7.60% and 8.64% at room temperature, respectively.

Table S6. The decay lifetimes of **DTST** in 2-MTHF (50.0 μM) at 530 nm measured at different temperature.

Temperature/K	τ (ms)
77	15.78
100	15.71
140	14.91
200	7.83
240	6.25
260	3.18×10^{-6}
280	3.08×10^{-6}
300	2.80×10^{-6}

Table S7. TPEF and TPA cross-sections of **DTST** sample and **LIFM-SHL-1** excited at 760/ 800 nm.

Sample	TPEF cross-sections (GM) 760 nm / 800 nm	TPA cross-sections (GM) 760 nm / 800 nm
DTST	3143.92 / 6956.16	41367.37 / 91528.42
LIFM-SHL-1	6820.64 / 13825.44	78309.78 / 160760.93

Table S8. TD-DFT calculated energy levels of **DTST**.

State	**Energy (eV)**	**Transition configuration**
S_1	2.21	H→L (99.2%)
T_1	1.84	H→L (91.0%)
T_2		H-2 → L (63.9%),

	2.22	H-11 →L (9.3%), H→L (7.0%), H→ L+1 (6.8%)
T_3	2.47	H-1→ L (97.8%)
T_4	2.81	H → L+1 (77.1%) H-2 → L (9.8%)
T_5	3.01	H → L+2 (48.5%) H-1 → L+1 (12.9%) H-3 → L+3 (6.2%)
T_6	3.11	H → L+3 (38.5%) H-1 → L+2 (14.3%) H-3 → L+2 (9.4%) H-2→ L+3 (6.3%)
T_7	3.14	H → L+4 (26.5%) H-1 → L+3 (14.2%) H-2 → L+2 (11.8%) H-3 → L (8.1%) H-3 → L+1 (7.3%)
T_8	3.15	H → L+5 (30.3%) H-1 → L+4 (13.6%) H-1 → L+2 (6.7%)
T_9	3.19	H-3→ L (81.5%)
T_{10}	3.33	H-4 → L (53.9%) H-2 → L (10.7%) H-8 → L (8.8%)

		H-10 → L (6.7%) H-11 → L (5.0%)

Table S9. TD-DFT calculated energy levels of **LIFM-SHL-1** fragments.

State	Energy (eV)	Transition configuration
S_1	2.27	H-3→ L (99.1%)
T_1	2.22	H → L+1 (94.8%)
T_2	2.28	H-1 → L (93.6%)
T_3	2.47	H → L (85.5%)
T_4	2.49	H → L+4 (30.7%) H-3 → L+1 (26.3%) H→ L (6.4%)
T_5	2.51	H-1→ L+2 (19.5%) H-8 → L (19.4%) H-4 → L (9.4%) H-1→ L+ (38.8%) H-26 → L (6.4%) H→ L (5.9%)
T_6	2.80	H-4→ L (50.5%) H-5 → L (21.4%) H-1 → L+2 (13.4%)
T_7	2.82	H-2 → L+1 (83.8%)
T_8	2.90	H → L+4 (46.7%) H-3 → L+1 (28.2%) H-5 → L+1 (5.3%)
T_9	2.94	H-8→ L (32.2%) H-1 →L+2 (29.6%)

		H-1→ L+3 (9.2%)
T_{10}	2.98	H-2 → L (94.3%)

Table S10. The decay lifetime of **LIFM-SHL-1** measured after soaking in base solution.

pH	τ_1 (ns)	A_1 (%)	τ_2 (ns)	A_2 (%)	τ (μs)
6.7	43.31	15.48	1651.97	84.52	1.40
8.0	56.10	17.03	1705.28	82.97	1.42
9.0	59.58	16.26	1745.07	83.74	1.47
10.0	69.48	15.52	1767.60	84.48	1.50
11.0	103.43	15.46	2240.96	84.54	1.91
12.0	114.8447	16.02	2390.314	83.98	2.03

REFERENCES

[1] Dolomanov, O. V.; Bourhis, L. J.; Gildea, R. J.; Howard, J. A. K.; Puschmann, H. OLEX2: a complete structure solution, refinement and analysis program. *J. Appl. Crystallogr.* **2009**, *42*, 339-341.

[2] Frisch, M. J.; Trucks, G. W.; Schlegel, H. B.; Scuseria, G. E.; Robb, M. A.; Cheeseman, J. R.; Scalmani, G.; Barone, V.; Mennucci, B.; Petersson, G. A.; Nakatsuji, H.; Caricato, M.; Li, X.; Hratchian, H. P.; Izmaylov, A. F.; Bloino, J.; Zheng, G.; Sonnenberg, J. L.; Hada, M.; Ehara, M.; Toyota, K.; Fukuda, R.; Hasegawa, J.; Ishida, M.; Nakajiama, T.; Honda, Y.; Kitao, O.; Nakai, H.; Vreven, T.; Montgomery, J. A., Jr.; Peralta, J. E.; Ogliaro, F.; Bearpark, M.; Heyd, J. J.; Borthers, E.; Kudin, K. N.; Staroverov, V. N.; Kobayashi, R.; Normand, J.; Rahavachari, K.; Rendell, A.; Burant, J. C.; Iyengar, S. S.; Tomasi, J.; Cossi, M.; Rega, N.; Millam, J. M.; Klene, M.; Knox, J. E.; Cross, J. B.; Bakken, V.; Adamo, C.; Jaramillo, Gomperts, R.; Stratmann, R. E.; Yazyev, O.; Austin, A. J.; Cammi, R.; Pomelli, C.; Ochterski, J. W.; Martin, R. L.; Morokuma, K.; Zakrzewski, V. G.; Voth, G. A.; Salvador, P.; Dannenberg, J. J.; Dapprich, S.; Daniels, A. D.; Farkas, O.; Foresman, J. B.; Ortiz, J. V.; Cioslowski, J.; Fox, D. J. Gaussian, Inc. Wallingford CT, 2009.

[3] Lu, T.; Chen, F. Multiwfn: a multifunctional wavefunction analyzer. *J. Comput. Chem.* **2012**, *33*, 580-592.

[4] Lu, T.; Chen, Q. Interaction Region Indicator: A Simple Real Space Function Clearly Revealing Both Chemical Bonds and Weak Interactions**. *Chemistry–Methods* **2021**, *1*, 231-239.

[5] Humphrey, W.; Dalke, A.; Schulten, K. VMD: Visual Molecular Dynamics. *J. Mol. Graphics* **1996**, *14*, 33-38.

[6] P. R. Spackman, M. J. Turner, J. J. Mckinnon, S. K. Wolff, D. J. Grimwood, D. Jayatilaka, M. A. Spackman, CrystalExplorer: a program for Hirshfeld surface analysis, visualization and quantitative analysis of molecular crystals. *J. Appl. Crystallogr.* **2021**, *54*, 1006-1011.

[7] G. Ferey, C. Serre, Large breathing effects in three-dimensional porous hybrid matter: facts, analyses, rules and consequences. *Chem. Soc. Rev.* **2009**, *38*, 1380-1399.

[8] Chen, G.; Zhou, Z.; Feng, H.; Zhang, C.; Wang, Y.; Qian, Z.; Pan, J. An aggregation-induced phosphorescence probe for calcium ion-specific detection and live-cell imaging in Arabidopsis thaliana. *Chem. Commun.* **2019**, *55*, 4841-4844.

[9] Wang, T.; Zou, Y.; Huang, Z.; Li, N.; Miao, J.; Yang, C. Narrowband Emissive TADF Conjugated Polymers towards Highly Efficient Solution-Processible OLEDs. *Angew. Chem., Int. Ed.* **2022**, *61,* e202211172.